Pergamon

Int. J. Solids Structures Vol. 32, No. 17/18, pp. 2793–2812, 1995
Copyright © 1995 Elsevier Science Ltd
Printed in Great Britain. All rights reserved
0020-7683/95 $9.50 + .00

0020-7683(94)00295-9

THREE-DIMENSIONAL ANALYSIS OF THE IMPACT FRACTURE OF 4340 STEEL

TIMOTHY PREMACK
NASA Goddard Space Flight Center, Code 751, Greenbelt, MD 20771, U.S.A.

and

ANDREW S. DOUGLAS
Department of Mechanical Engineering, The Johns Hopkins University, Baltimore, MD 21218, U.S.A.

(*Received* 3 *February* 1994)

Abstract—An analysis of the impact fracture of a three-point-bend specimen made of 4340 steel is performed using the finite element method (FEM). In the experiments performed by Sharpe *et al.* [(1988) *WNS/ASD*-88-02. The Johns Hopkins University Baltimore, Maryland] the crack tip opening displacement (CTOD) 100 μm behind a prefatigued crack tip was measured. The numerical analyses performed to model this experiment used a three-dimensional mesh which accounted for crack curvature and examined the role played by the residual plastic deformation as a result of the precracking procedure and also the role played by material rate sensitivity of the flow stress. The finite element simulation which included both precracking and strain rate sensitivity effects modeled the CTOD well for the observed 10 μs. From this model, local stress and deformation fields can be assessed. These indicate a significant increase in the impact fracture toughness over the quasi-static toughness. Error estimates and other observations for experimentalists are made, based on different FEM simulations.

1. INTRODUCTION

1.1. *Background*

The determination of the static fracture toughness has been defined by the ASTM E 399 specification (American Society of Testing and Materials, 1983). However, the determination of the dynamic fracture toughness, at rates in excess of 1×10^5 MPa m$^{1/2}$ s^{-1}, continues to be under development. The difficulty in dynamic tests is the determination of the fracture toughness from experimental observations and measuring the time at which the crack initiates. Some fracture experiments have been designed to facilitate their use of simplified analyses, including a quasi-static assumption (Hackett *et al.*, 1987) and a single stress wave analysis (Ravichandran and Clifton, 1989), while others require a fully dynamic analysis (Douglas and Suh, 1990; Premack and Douglas, 1993). The techniques for determining fracture initiation include changes in a strain gage signal close to the crack tip (Yokoyama and Kishida, 1988), A/C potential drop described by Giovanola (1985), distorted caustic (Zehnder and Rosakis, 1990), a comparison of the observed and modeled fracture specimen behavior (Douglas and Suh, 1990) and the use of the (quasi-static) ASTM E 399 procedure in dynamic fracture. For ductile materials the J-integral is used to quantify fracture toughness (Kanninen and Popelar, 1985).

When the time between the onset of loading and fracture initiation is long enough, stress wave effects will no longer be dominant and a quasi-static analysis may be used to relate the remote loading to the near-crack tip parameters. For a drop tower loaded three-point-bend (3PB) beam—such as those experiments performed by Hackett *et al.* (1987)—Nakamura *et al.* (1986a) quantified this critical time and showed that the J-integral derived by Merkle *et al.* (1973) can be calculated from remote measures of load and crack mouth opening displacement (CMOD). Costin *et al.* (1976) used an explosively generated single tensile stress wave to load an annularly precracked round bar with a single tensile stress wave at the cracked section. The load at the section was determined from upstream and

downstream strain gages, while the CMOD was measured using a moiré-based displacement gage. Initiation was determined by the ASTM E 399 5% offset method and also by a change in the shape of the reflected stress wave. The J-integral was computed from a quasi-static expression derived by Merkle *et al.* (1973) and numerically verified as being appropriate for the dynamic loading in this experiment by Nakamura *et al.* (1985a). Zehnder and Rosakis (1990) used the method of caustics in drop tower loaded 3PB specimens of 4340 steel. Numerically generated caustics from a quasi-static, three-dimensional finite element model were used to interpret the local stress state from the observed caustics, while the change in the shape of the caustic was used as an indicator of crack growth. Loading rates for these methods are on the order of 1×10^6 MPa $m^{1/2}$ s^{-2}.

Loading a static crack by a single stress wave facilitates the use of expressions for the local fields in terms of the magnitude of the load step derived by Thau and Lu (1971) or Lee and Freund (1990), or simplifies the numerical analysis by reducing the model size. Where the geometry or the loading is not well approximated by the ideal conditions assumed for these expressions, the finite element or difference method may be used to compute the stress intensity factor or J-integral. Ravichandran and Clifton (1989) modeled the impact loading (by means of a plate impact facility) of a thin precracked disk as a single tensile stress wave impinging on a semi-infinite crack using the finite difference method. Loading rates were on the order of 1×10^8 MPa $m^{1/2}$ s^{-1}. The experiment and analysis include fracture initiation, crack growth and arrest and yield the energy release rate during propagation. Homma *et al.* (1983) used a linear elastic, plane-stress finite element model of a single edge notched specimen to determine the stress intensity factor by modeling the applied load as a single tensile wave applied to the crack face. Initiation was determined by applying successively greater loads until fracture was detected optically.

Numerical methods have been used when neither of the two previous methods (quasi-static assumption and single stress-wave loading) are applicable. Krishnaswamy *et al.* (1988) used a dynamic, three-dimensional finite element analysis of a drop tower loaded 3PB specimen of 4340 steel to generate caustics from which one could determine the local fracture parameters by observing the caustics generated in their dynamic experiments. Input loads to the analysis were taken from an instrumented load tup, while fracture initiation was assumed to occur when the observed caustic changed shape, indicating a change in the character of the local deformation field. Kobayashi and Yung (1988) used remotely measured loads as input to a finite element analysis of a drop tower loaded 3PB specimen of an alumina ceramic in crack propagation tests. Yokoyama and Kishida (1988) used the remotely measured applied and support loads as input to a finite elment analysis of drop tower loaded 3PB specimens of aluminium and titanium alloys, with loading rates on the order of 1×10^6 MPa $m^{1/2}$ s^{-1}.

1.2. *Present work*

Sharpe *et al.* (1988) and Tregoning *et al.*, (1992) used the interferometric strain displacement gage (ISDG) to measure the crack tip opening displacement (CTOD) 100 μm behind the surface crack tip in quasi-static and impact loaded 3PB specimens of 4340 steel and HY100 steel. These tests are described in the next section.

In order to obtain fracture toughness measures, these investigators assumed that the observed CTOD is a direct measure of the stress intensity factor, regardless of loading rate, and that the loading rate was constant during the dynamic experiment. The quasi-static fracture tests were used to obtain a CTOD versus *load* curve to interpret the dynamic CTOD versus *time* curve. Fracture initiation was determined using the ASMT E 399 5% offset method. Using the quasi-static results to obtain the local fracture parameters from the observed CTOD requires that the static and dynamic fracture specimens be similarly precracked and that the material is strain-rate insensitive. In order to evaluate the validity of the Sharpe and Tregoning assumptions, Douglas and Suh (1990) performed rate sensitive, elastic–plastic, two-dimensional finite element analyses of the dynamic experiments on HY100. The objective of the analysis was to correlate the observed and computed CTOD values up to the onset of fracture. The results of the analysis were then used to compute the J-integral numerically. Since crack growth was not modeled, the observed CTOD values

should have become larger than the calculated CTOD values at a time corresponding to crack extension. If the fidelity of the finite element model was sufficiently high, the point where the two curves diverged should indicate crack growth. However, because the pre-cracking procedure (which gives rise to residual plastic stresses at the crack tip) was not modeled, the initial 4 μs of the calculated CTOD versus time curve did not match the observed data.

Premack and Douglas (1993) extended the analysis to include these precrack effects. The analysis method used the load point displacement from a coarse three-dimensional impact model and applied it to a refined two-dimensional plane stress model which accounted for the residual stress state due to cyclic fatigue precracking. The observed and computed CTOD versus time curves were within 10% for the HY100 steel. However, the plane stress model exhibited too much closure in quasi-static analyses.

The purpose of this paper is to investigate the ability of a numerical simulation of the experimental method of Tregoning *et al.* (1992) to determine the dynamic fracture toughness of ductile materials. This paper extends the work by Douglas and Suh (1990) and by Premack and Douglas (1993) by using a dynamic, three-dimensional analysis with a finite element model having the resolution necessary to obtain the CTOD. Specific features of the experiment are investigated, including the sensitivity to different measurements and the effect of rate sensitivity. Also examined is how the analysis can guide further experiments.

2. FRACTURE EXPERIMENTS

2.1. *ISDG method*

The ISDG developed by Sharpe (1970) used the interference pattern produced by the illumination of two small reflective indents with coherent light (Fig. 1) to determine the distance change between these two indents. The interference pattern oscillates from bright to dark, as observed from a stationary point P_1, as d, the distance between the indents, changes. By observing the fringe patterns from two locations, P_1 and P_2, rigid body motions in the y-direction can be eliminated by averaging the changes in fringe intensity. The change in the distance between the indents is

$$\delta d = \frac{\delta M_1 + \delta M_2}{2} \frac{\lambda}{\sin \alpha_0}, \tag{1}$$

where δM_1 and δM_2 are the changes (bright to dark) in the fringe intensity as observed

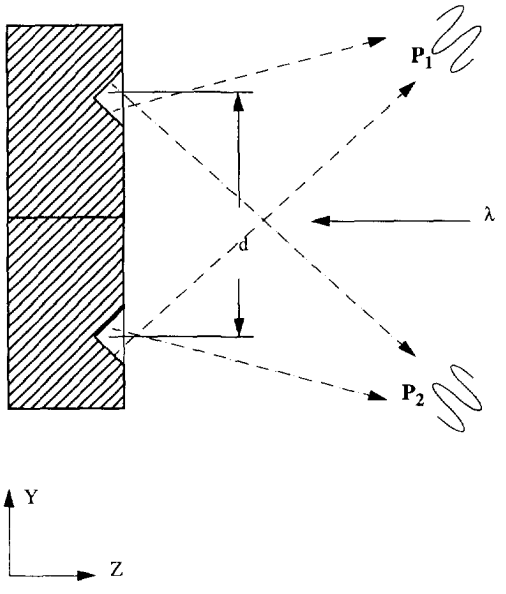

Fig. 1. A schematic of the interferometric strain displacement gage.

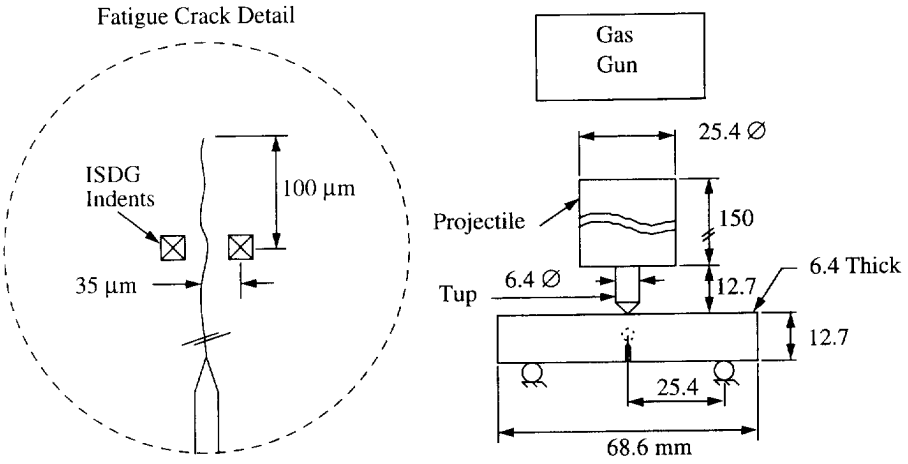

Fig. 2. The dynamic three-point bend beam experiment. Inset is shown the location of the ISDG indents. A Teflon ring (not shown) was used to hold the tup in place.

from P_1 and P_2, λ is the wavelength of the coherent light source and α_0 is the angle between the light source and the indent surface. The ISDG indents were formed in the specimen using a Vickers hardness tester with a pyramid-shaped diamond stylus. The fringe intensities are recorded using photomultiplier tubes connected to a digital oscilloscope. A He–Ne laser with $\lambda = 0.6329$ μm and $\alpha_0 = 47$ was used, which results in a 0.5 μm resolution in CTOD.

2.2. *Fracture tests*

The quasi-static tests followed the standard ASTM E 399 procedure. Precracked 3PB specimens of 4340 steel were subjected to quasi-static loading. The specimen dimensions are shown in Fig. 2 while the chemical and physical properties are provided in Tables 1 and 2, respectively. Results of the quasi-static fracture test are shown in Table 3—note that the specimen dimensions are adequate for a valid plane-strain fracture test.

The impact fracture tests used specimens of the same dimensions and preparation as in the quasi-static tests. The dynamic load was applied by an aluminum cylindrical projectile (with a mass of 52 g) traveling at a nominal velocity of 45 m s^{-1}, which impacts a hardened steel tup held in place against the specimen by a Teflon ring (Fig. 2). The CTOD data were recorded after the distance between the indents increased by 0.5 μm. To determine the projectile's speed, its trajectory crossed the optical path between two photodiodes located

Table 1. Chemical composition of 4340 steel (percentage)

C	Mn	Si	S	P	Ni	Mo
0.41	0.8	0.24	0.004	0.012	1.85	0.22

Table 2. Mechanical properties of 4340 steel

Elastic modulus (GPa)	0.2% yield stress (MPa)	Hardness (R_C)	Density (kg m^{-3})	Poisson's ratio
226	1530	52	7.88×10^3	0.291

Table 3. Quasi-static fracture test results (Sharpe and Shapiro, 1988; Tregoning *et al.*, 1992)

Test number	Crack length (mm)	P_q (kN)	K_q (MPa $m^{1/2}$)	Valid (K_{Ic})	J-integral (kPa m)	Valid (J_{Ic})
COD 14	6.41	3.38	51	Yes	11	Yes

at a known distance and a laser. The speed was determined by measuring the time interval between the change in the output of each photodiode.

3. FINITE ELEMENT ANALYSIS

3.1. *Overview*

One difficulty in obtaining finite element results which replicate the observed (quasi-static) CTOD is that the specimen has been precracked, resulting in an asymmetric, curved crack front (see Fig. 3) and residual stresses on the crack faces. Because the CTOD is measured 100 μm from the surface crack tip while the crack curvature, the difference between the surface and center-line crack lengths, is on the order of 5% of the specimen thickness, this measurement is sensitive to the crack curvature. Additionally, since the indents are placed in the wake of the fatigue precrack, the CTOD will be influenced by the residual plastic stresses due to crack closure. A quasi-static analysis that does not model the closure will exhibit a greater CTOD at a given load than the observed CTOD. Similarly, a dynamic analysis that ignores the precrack closure effects will result in a crack which opens prematurely. This difference in the time corresponding to the onset of crack opening is important because the local stress fields increase rapidly with time and also because the experiment used a 0.5 μm change in the CTOD to trigger the onset of data collection.

The three-dimensional finite element analyses presented here model both the curved crack front and the residual stress state. Analyses with different crack lengths and which ignore the precrack effects are also run to demonstrate their effects on the local crack tip fields. In addition, analyses are performed to determine the sensitivity of the CTOD to measurement location, material properties, projectile speed and tup geometry. These analyses provide error estimates for the fracture toughness (the J-integral) and can be used to guide further experiments. The finite element programs NIKE3D (Maker, 1991) and DYNA3D (Whirley, 1991) from the Lawrence Livermore National Laboratory (LLNL) are used to perform the quasi-static and dynamic analyses, respectively. INGRID (Christon and Dovey, 1992), a preprocessor, prepares the input files for NIKE3D and DYNA3D. Taurus (Spelce, 1991) is a post-processor, which displays the results graphically. NIKE3D is a three-dimensional, implicit, non-linear finite element code, while DYNA3D is a three-dimensional, explicit, non-linear finite element code both of which account for finite deformations and large displacements. DYNA3D uses the central difference method to integrate

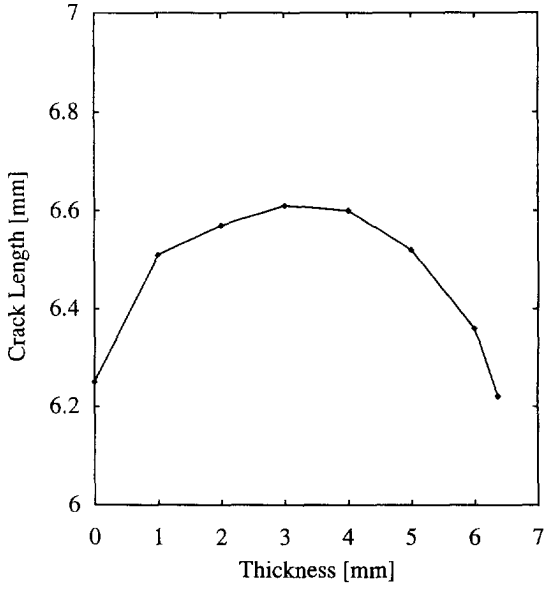

Fig. 3. The crack length versus thickness for the dynamically loaded 4340 steel specimen. The curvature produced by precracking appears more pronounced than it actually is due to scale differences.

the equations of motion (Belytschko, 1983). Because the central difference method is only conditionally stable, DYNA3D automatically adjusts the integration time step each iteration. One particularly important feature of the codes is the ability to pass a statically initialized model from NIKE3D to DYNA3D. All programs are executed on a Sun Sparc Station 10 model 41 with 128 Mbyte of RAM and 4 Gbyte of disk space.

3.2. *J-integral*

The J-integral, or non-linear energy release rate, proposed by Rice (1968), has been shown to characterize the fracture toughness of materials by Begley and Landes (1972). The J-integral is used for ductile materials when the restrictions imposed on the fracture toughness by linear fracture mechanics assumptions requires an impractical specimen size. For materials obeying the Ramberg–Osgood material law, the J-integral has been shown to be the amplitude of the Hutchinson, Rice and Rosengren (HRR) field singularity (Hutchinson, 1968; Rice and Rosengren, 1968). The path independence of the J-integral requires that the material be loaded monotonically and proportionally where deformation theory plasticity holds. The J-integral has been extended to include inertia forces, body forces and thermal effects by Aoki *et al.* (1980, 1984), Atluri (1982) and Nakamura *et al.* (1985b). It has also been extended to three dimensions to provide a point-wise evaluation of the J-integral along the crack front (deLorenzi, 1982; Sakata *et al.* 1983).

The J-integral is computed numerically using the method of virtual crack advance developed by Parks (1977) and Hellen (1975). The average value of the J-integral without crack-face tractions, thermal effects or body forces is

$$J = \int_V \left[\sigma_{ij} \frac{\partial u_i}{\partial x_k} \frac{\partial q_k}{\partial x_j} - U \frac{\partial q_k}{\partial x_k} + \rho \frac{\partial^2 u_i}{\partial t^2} \frac{\partial u_i}{\partial x_k} q_k \right] \mathrm{d}A, \tag{2}$$

where V is the domain surrounding the crack front, σ_{ij} is the stress, u_i is the displacement, ρ is the mass density, U is the strain energy density, t is time and q_i is the virtual displacement. Lowercase subscripts indicate a summation from one to three. The virtual displacement q_i must be unity on the crack front, zero on the boundary and differentiable in the domain. Shih *et al.* (1986) performed numerical tests using two virtual displacement functions: the plateau function having unity inside the boundary and zero on the boundary and the pyramid function having unity on the crack tip, zero on the boundary and linearly interpolated for positions in-between. They found the two functions to have little effect on the values of the J-integral.

Equation (2) is integrated numerically over all the elements in the domain using a J-integral post-processor from the Lawrence Livermore National Laboratory which was modified to perform dynamic calculations. The plateau function is used to calculate the virtual displacements. The integrand is evaluated at the centroid of each element, while the field quantities are obtained from the Taurus plot files produced by NIKE3D and DYNA3D analyses. For the quasi-static analyses, the strain energy density is integrated in the J-integral post-processor, while for the dynamic analyses the strain energy is obtained directly from DYNA3D.

3.3. *Precrack Modeling*

The finite element method has been used to simulate fatigue cracks by Kobayashi *et al.* (1973), Andersson (1975) who modeled growing cracks, and Newman (1976) who simulated the crack closure caused by a growing cyclically loaded crack. McClung and Sehitoglu (1989a,b) performed numerical tests to determine the sensitivity of the mesh size around the crack tip on the crack closure loads for two-dimensional, plane-stress models using four-node bilinear elements. They suggested that the crack growth distance be less than 0.10 times the plastic zone radius in front of the crack tip at maximum load.

3.4. *Finite element analysis of fracture tests*

The 3PB specimen is modeled using 8000 eight-node brick elements (Fig. 6). The model is used in both the quasi-static and dynamic analyses. Symmetry about the xy-plane and

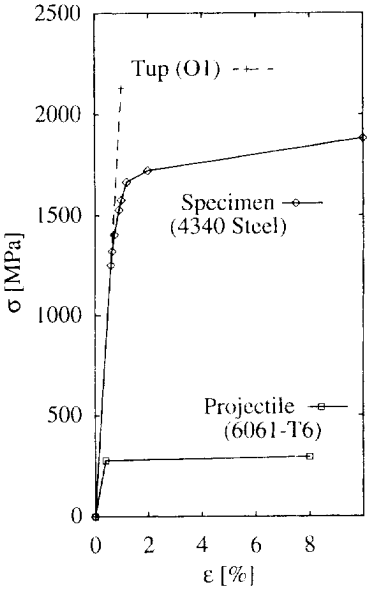

Fig. 4. The uniaxial stress strain curves for 4340 steel, projectile and tup.

yz-plane allowed for modeling only one-quarter of the specimen. The model has four layers of elements parallel to the xy-plane with normalized z locations of 0.0, 0.48, 0.90, 0.97 and 1.0. Nodal spacing around the crack tip was 25 μm to capture the CTOD at the indents. Because the actual specimen is precracked, it contained a curved crack front. The curvature was measured (Fig. 3) and modeled. A focused mesh, where crack tip elements are collapsed to wedges, is not used because the precrack was modeled. The 3PB specimen support was modeled using a block with a sliding surface that allowed for separation.

The quasi-static analysis uses only the 3PB model described above in which the elements have trilinear interpolation functions with constitutive equations solved at the eight Gauss points. The 4340 steel is modeled as elastic plastic using the J_2 incremental plasticity material model with isotropic hardening. The stress–strain curves (Fig. 4) were obtained from uniaxial tension tests (Shapiro, 1987). The plastic portion of the 4340 curve is input to NIKE3D pointwise as the stress versus the effective plastic strain, while the Broyden–Fletcher–Goldfarb–Shanno (Matthies and Strang, 1979) option in NIKE3D is used to solve the non-linear analysis. The experimental load is modeled with a uniformly distributed nodal load applied over an area 1 mm long by the beam thickness. For completeness, the quasi-static finite element simulations continue to load the specimen to ~120% of the maximum experimentally applied load.

The experimental precracking procedure is modeled by growing a crack from the straight notch to the (observed) curved crack front, a distance of approximately 1.2 mm, by sequentially releasing the nodes of 16 crack fronts while adjusting the load based on the actual fatigue loads. The loads are not cycled, as was performed experimentally, since this was beyond the computational limits of the combined software and hardware. The crack growth increment for the final 225 μm of crack length was $\Delta a = 25$ μm. The forward length of the plastic zone in front of the crack tip is approximately 125 μm at full load. While the crack growth increment is larger than that suggested by McClung and Sehitoglu (1989b) for two-dimensional, bilinear, plane stress elements, finite element tests showed that nodal spacing less than 25 μm caused little change in the CTOD curves for non-precracked quasi-static and dynamic models. Once the crack is grown, the applied load is reduced to 10 N and the current stress and displacement state is written to the DYNA3D initialization file. The precracking takes about 100 load increments using 60 h of CPU time, 200 Mbyte of disk space and 90 Mbyte of RAM.

The dynamic analyses model the experiment using the beam described above together with a 2000 element tup and 2000 element projectile. The elements use trilinear functions to interpolate the displacements and have constitutive equations solved at their centers.

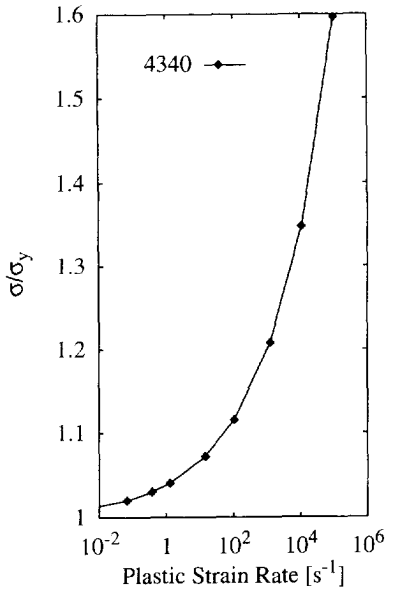

Fig. 5. The normalized effective stress versus plastic strain rate for 4340 steel.

DYNA3D uses a kinematic viscosity to control element hourglassing. The default value of 0.1 is used. The observed projectile velocity of 43.82 m s^{-1} is used as the initial condition for the finite element simulations. The tup is modeled as linearly elastic and projectile as elastic–plastic. The 4340 steel is modeled as elastic–plastic with isotropic hardening. The plastic portion of these curves is input to DYNA3D pointwise as the universal stress strain curve (Fig. 4). While 4340 is relatively rate insensitive (Syracuse University Research Institute, 1963), both rate insensitive and rate sensitive models are run. The relate sensitivity is modeled by providing the normalized yield stress versus plastic strain rate in pointwise form (Fig. 5). Contact surfaces between the projectile and the tup, tup and the beam, crack face and stone wall and the beam and the support are modeled as frictionless.

A typical dynamic analysis of 18 μs requires approximately 5 h of CPU time using 150 Mbyte of disk space. The time step ranged from 3.0 to 2.3 ns, with a total of 7000 time steps with state data written every 0.2 μs.

4. RESULTS AND OBSERVATIONS

4.1. *Quasi-static*

The objective of the finite element analysis of the quasi-static fracture toughness experiment is to obtain CTOD values which correlated well with the observed CTOD versus load curves, up to the onset of fracture. If the numerical simulation is able to produce a CTOD versus load curve that is close to the experimentally observed curve, then this verifies that the material model, simulation of the precracking procedure and mesh are appropriate. The CTOD versus load responses for the precracked and non-precracked finite element models and the quasi-static observed data are shown in Fig. 7. The CTOD as observed and computed for the precracked model correlate very closely up to 2.0 kN, after which the observed CTOD values become larger. At the critical load of 3.38 kN (Table 3) at which, according to the ASTM E 399 procedure, fracture initiation occurs, the observed CTOD curve deviates significantly from the precracked model curve.

The non-precracked finite element model (Fig. 7) provides an upper bound to the CTOD versus load curve before fracture initiation, since there is no closure effect. The effect of the residual plastic stress state due to the prepacking procedure on the CTOD vanishes at about 2.1 kN, where the precracked and non-precracked CTOD versus load curves are essentially parallel. The smaller CTOD for a given load in the precracked model is due to the residual plastic deformation, which was first observed by Elber (1970), which provides a closure stress retarding the crack opening.

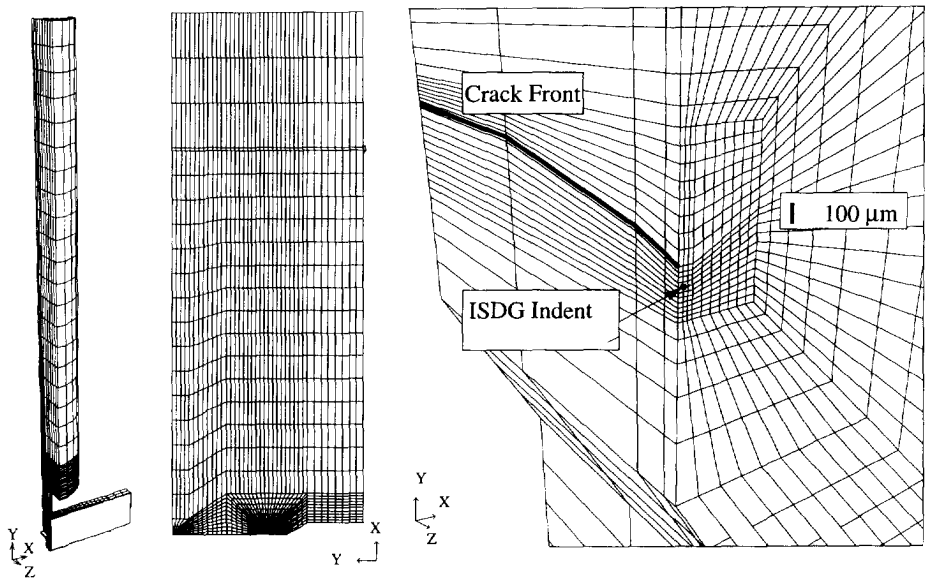

Fig. 6. Three-dimensional finite element model of the dynamic fracture experiment. The model of the beam was used in the quasi-static and dynamic analyses. The detail of the crack tip shows the curved crack front and location of the ISDG indent.

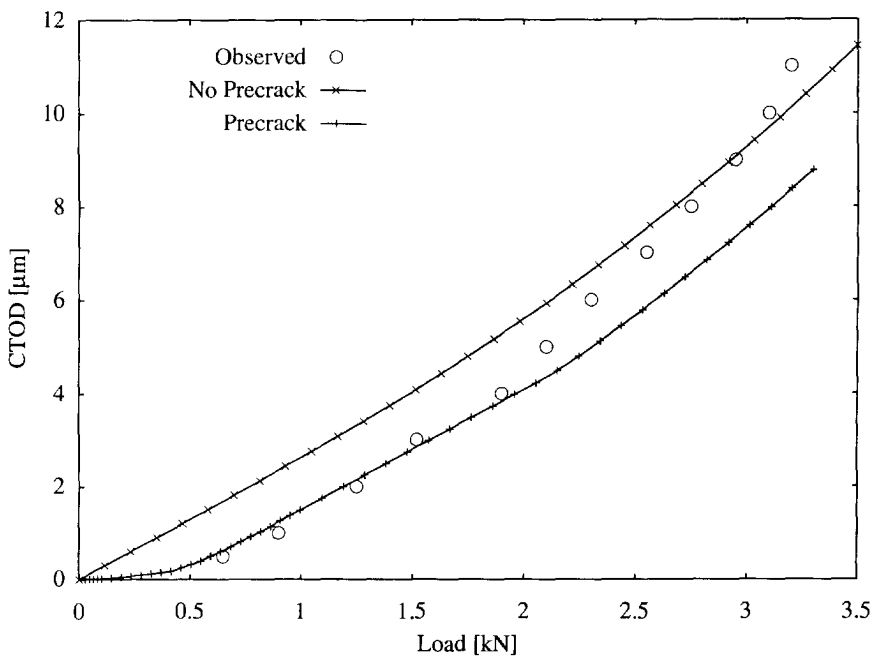

Fig. 7. The quasi-static CTOD versus load for observed and precracked and non-precracked quasi-static analyses. LEFM predicts a P_q of ~3.1 kN.

Using the load of 2.0 kN as the point of deviation between the observed and computed CTOD versus load responses as an indication of fracture initiation, the J-integral is approximately 4.0 kPa m, which is about 64% less than the plane strain derived value of 11 kPa m (Table 3). The divergence of the observed and precracked model CTOD versus load curves could be caused by the crack extending or by modeling deficiencies. At indent locations ± 25 μm (from the nominal 100 μm behind the surface crack tip) the CTOD versus load response is $\pm 20\%$ of the CTOD computed using the location at 100 μm (see Fig. 8). Figure 8 therefore shows the sensitivity of the CTOD to a change in crack length or an error in modeling the indent location with respect to the crack tip. A crack growth of 25 μm (see Fig. 7) in the load range from 2.0 to 3.0 kN would produce a new CTOD versus load curve

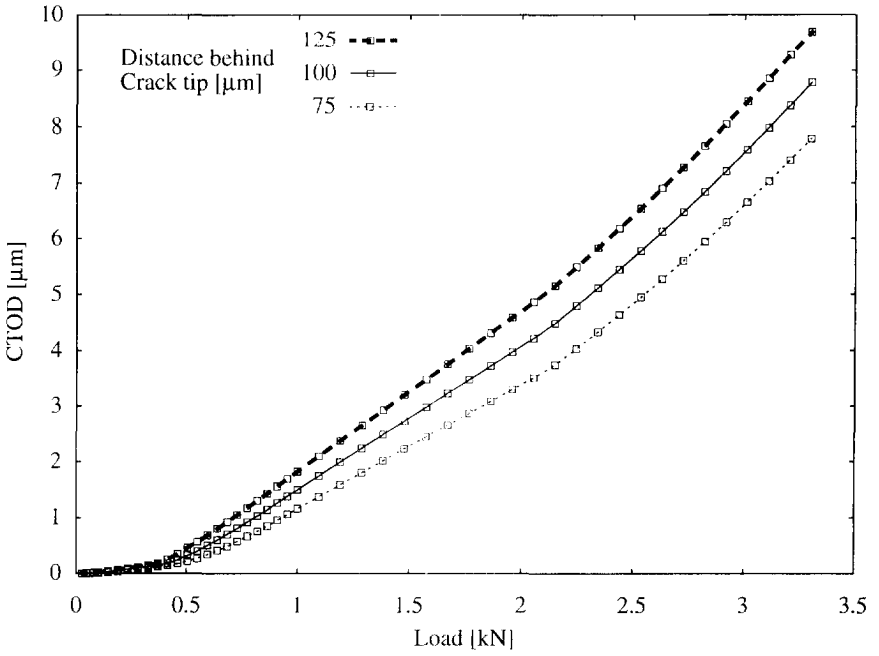

Fig. 8. The CTOD, as measured at three different locations behind the crack tip, versus load for the quasi-static precracked model.

with approximately the same slope as the observed CTOD versus load curve. However, the initial deviation at 2.0 kN is most probably due to the model not capturing the deformations at the crack tip accurately, since this load corresponds to the point at which the plasticity around the crack tip becomes significant. In either case, there is a close agreement between the observed and precracked models in the 0.0–2.0 kN range. This indicates that, at least for local stress conditions analogous to a load of less than 2.0 kN, the finite element mesh and modeling of the precrack is appropriate. This means that these features can reliably be used in a dynamic analysis. However, any dynamic analysis will require a strain-rate dependent material law to describe the elastic–plastic behavior of the 4340 steel.

4.2. *Dynamic analysis*

Four different finite element simulations of the dynamic fracture test are compared with the observed dynamic CTOD versus time response. The simulations are: with and without a precrack; and with and without material strain-rate sensitivity. The data are plotted with respect to two different times, normalized and experimental. In the finite element analysis, time begins ($t = 0$) when the projectile impacts the tup. Normalized time (Nakamura *et al.*, 1986a) is computed from this analysis time, by shifting time zero to the instant that the stress waves have propagated through the tup and the tup impacts the beam, and then normalized by c_1/h, where $c_1 = \sqrt{(E/\rho)}$ is the longitudinal wave speed, E is the modulus of elasticity, ρ is the mass density and h is the height of the specimen. This normalized time is used to compare each of the four different finite elemental models presented here and allows comparison of these results with other experiments and analyses in the literature. Experimental time, measured in microseconds, begins when the CTOD reaches a value of 0.5 μm, which was the value used in the experiment to trigger data collection.

The major result of each of the four finite element analyses (with and without a precrack and with and without strain-rate sensitivity) is the CTOD versus time. A comparison of the four different computed CTOD versus experimental time curves and the observed CTOD versus time response is given in Fig. 9. The rate sensitive prepacked model correlates very well with the observed data. There is no significant difference between these two curves, indicating that fracture initiation was unlikely during the time that the CTOD was recorded. Assuming that fracture did not occur before 10 μs, the dynamic fracture toughness of this

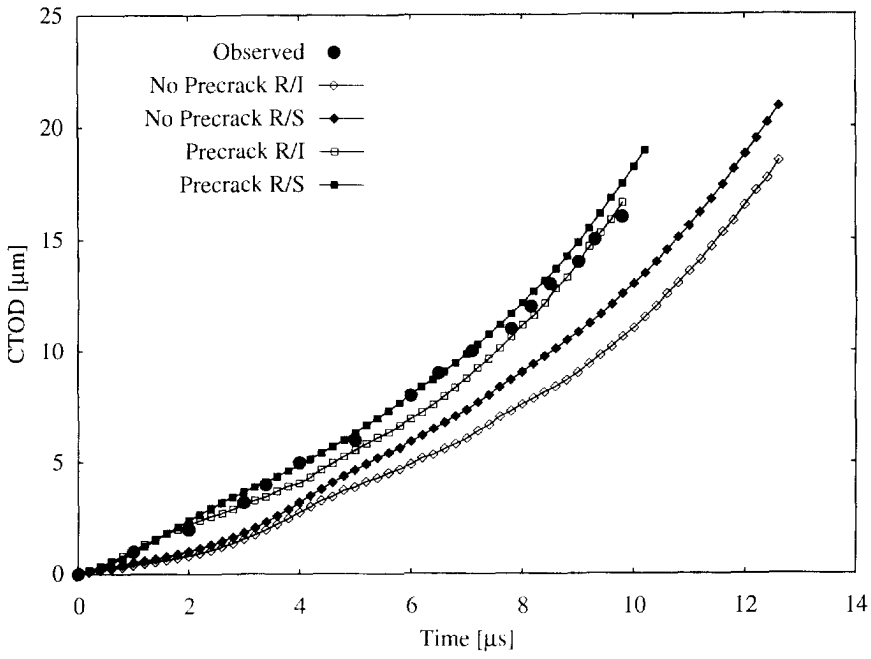

Fig. 9. The dynamic CTOD versus experimental time (microseconds) as observed, and as calculated from four models assuming a strain-rate sensitive and strain-rate independent material response and with and without a precrack. The precracked strain-rate sensitive model is in close agreement with the observed data. There is no indication of fracture initiation during the observed time interval ($0 < t < 10$ μs).

4340 steel is at least 25 kPa m (see also Fig. 12) compared with an ASTM E 399 derived quasi-static fracture toughness of approximately 11 kPa m (see above). The fracture toughness appears to be rate sensitive. The increase in the fracture toughness of AISI 4340 VAR steel has been noted by Zehnder and Rosakis (1990), Chi *et al.* (1989) and Godse *et al.* (1989).

The necessity for modeling the precracking procedure, which results in residual plastic strains local to the crack tip, is demonstrated in Fig. 10, where the CTOD versus normalized time for the four models is shown. The precracked models (both rate sensitive and rate independent) open at $\sim 1.1\ tc_1/h$, later than both the corresponding non-precracked models. The precracking procedure has no effect on the J-integral, as shown in Fig. 11, where the J-integral versus normalized time for each of the four models is shown.

The difference between the CTOD versus experimental time and normalized time can be seen by comparing Figs 9 and 10. In Fig. 9, the CTOD is plotted versus experimental time, that is in microseconds, beginning when the CTOD is 0.5 μm. In Fig. 10, the same CTOD values are plotted versus normalized time which beings when the tup impacts the beam. This is also evident in comparing Figs 12 and 11. While it is clear from Fig. 11 that the J-integral is independent of the precrack procedure, in Fig. 12 the time shift (imposed by the experiment) obscures the fact that both of the rate sensitive models (closed symbols) and both of the rate independent models (open symbols) have J-integral versus time responses which are indeed identical.

The effects of the material strain-rate sensitivity on the response of the fracture specimen are considered next. The dynamic load applied by the tup to the beam is shown in Fig. 15. At around $0.7\ tc_1/h$, the strain-rate effects at the load point become significant and the dynamic load on the rate sensitive model begins to exceed the load on the rate independent model. At around $4\ tc_1/h$, the material at the load point can no longer support an increase in load in both the rate sensitive and rate independent models. A maximum load of 35 kN is achieved for the rate sensitive model, which is about 15% greater than the maximum load on the rate independent model. The strain rates around the crack tip are on the order of $10^4\ s^{-1}$, giving rise to approximately a 30% increase in the local flow stress which would tend to decrease the deformations, in particular the CTOD. However, in Fig. 9, the

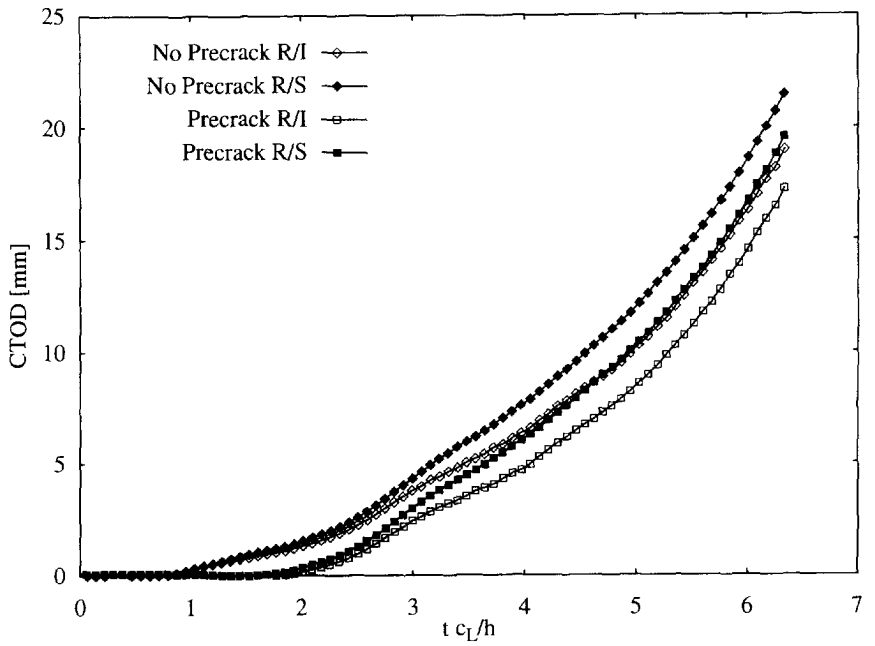

Fig. 10. The dynamic CTOD versus normalized time (four models). The precrack delays the crack opening by $\sim 1.1\ tc_L/h$

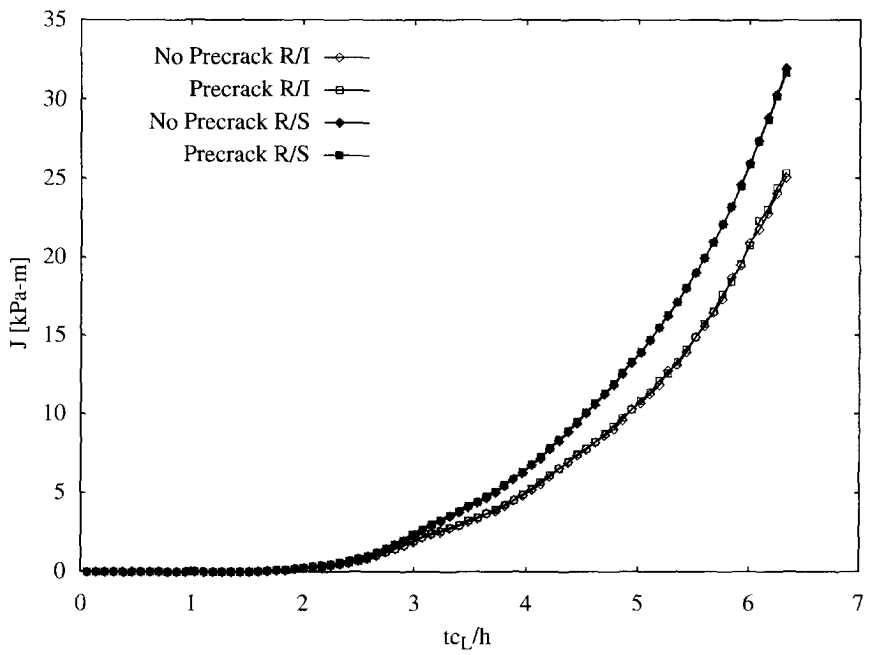

Fig. 11. The J-integral versus normalized time (four models). The J-integral is not affected by the precrack stresses, but the rate of change of the J-integral is higher for the rate sensitive than the rate insensitive models.

CTOD computed for the rate sensitive material is greater than that computed for the rate independent material model. This is because the rate sensitive model provides greater stiffness at the point of load application, transmitting more load into the specimen, resulting in an increase in the CTOD. While the computed CTOD (versus experimental time) for the rate sensitive model is about 10% greater than the CTOD for the rate independent model,

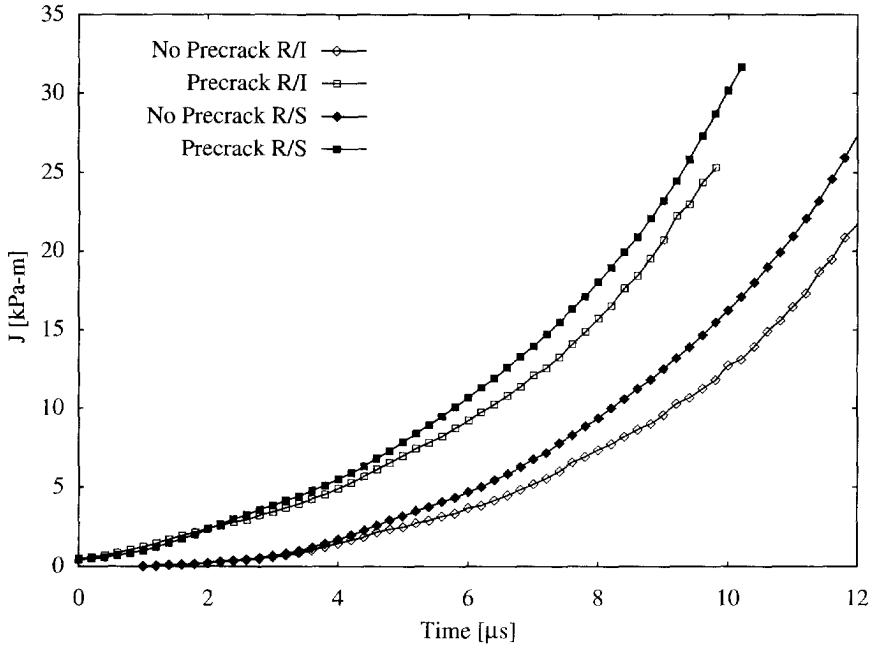

Fig. 12. The J-integral versus experimental time (four models). The precracked models produce a greater J-integral because the load transfer to the crack tip is greater.

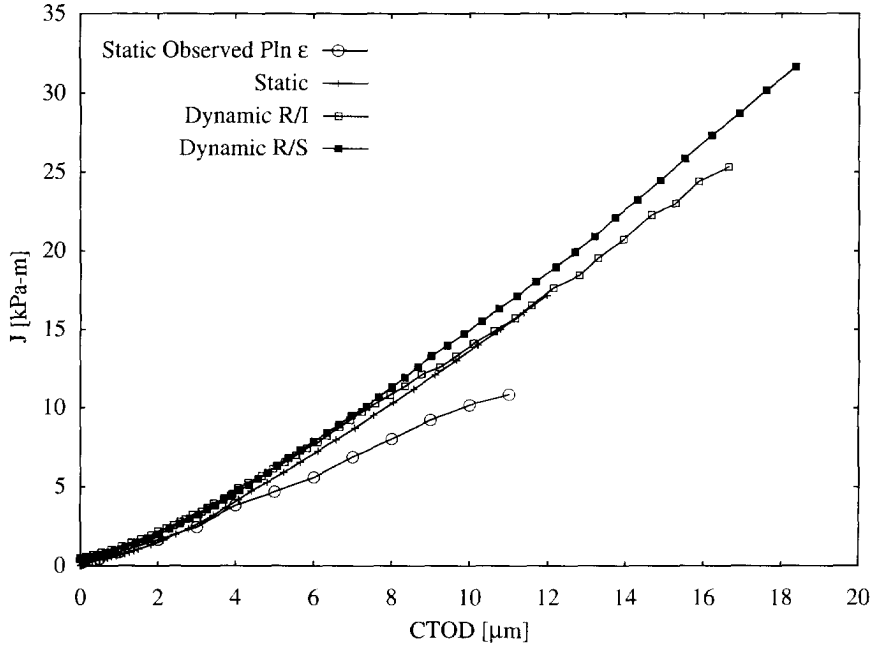

Fig. 13. The J-integral versus CTOD for observed, precracked quasi-static and precracked dynamic, strain-rate sensitive and strain-rate independent analyses. The linearity of the curves after 4 μm demonstrates that the CTOD is measured in the J-dominant region.

the increase in the J-integral for the rate sensitive model is about 25% over the rate independent model (after 6 μs) as shown in Fig. 12.

The validity of using a quasi-static J-integral versus CTOD curve to obtain the fracture toughness from the observed CTOD in a dynamic experiment is examined in Fig. 13. The J-integral is plotted versus CTOD for three precracked models—quasi-statically loaded,

dynamically loaded rate sensitive and rate independent models as well as the J-integral based on plane strain and plane stress using the observed loads from a quasi-static fracture test. Comparing the quasi-static and dynamic models with a rate independent material response, the J-integral versus CTOD response is within 8%. This means that, for rate insensitive materials, the CTOD observed in a dynamically loaded experiment may be used to determine the local fracture toughness (to within 10%) through the value of the static J-integral which corresponds to the CTOD. Reasons for the 8% difference between the quasi-static and rate independent dynamic responses include the effect of differences in their T-stress (see below).

The differences between the J-integral based on plane strain and plane stress (open circle symbols) and the precracked quasi-static (plus sign symbols) J-integral versus CTOD curves starting at about 5.0 μm (Fig. 13) are caused by the precracked quasi-static analysis not matching the observed response after 5.0 μm (Fig. 7).

In Fig. 13, for CTODs exceeding 6 μm, the slope of the J-integral versus CTOD response produced by the rate sensitive model is larger than any of the other models. Since this difference exceeds 15%, rate sensitive material behavior would preclude the use of any quasi-statically derived value of the toughness from the CTOD. Also, there is an apparent increase in the dynamic fracture toughness above the static initiation toughness independent of whether or not the material is modeled as rate sensitive or not. This can also be seen by comparing the maximum CTOD observed in a quasi static test of 11 μm (Fig. 7), with that observed in a dynamic test of 16 μm (Fig. 9).

A critical issue with fracture tests is that measurements be made such that the crack tip fields can be determined directly. In the impact fracture tests discussed, the test ends before the critical transition time after which remote measures of load define the local stress fields (Nakamura *et al.*, 1986b). The kinetic energy is monotonically increasing (Fig. 18) throughout the test so remote measures of load cannot be used to determine the fields local to the crack tip. However, the use of the CTOD does provide a direct measure of the J-integral as shown in Fig. 13. The CTOD, as defined by Tracy (1976), was shown by Shih (1981) to be linearly related to the J-integral. Tracy's definition of the CTOD can also be shown to be linearly related to the J-integral using the Dugdale strip yield model. In the experiments being discussed here, neither of these analyses are valid since the HRR-dominated region does not engulf the location of the indents and because the material does strain harden. However, as shown in Fig. 13, the observed CTOD versus J-integral response is linear after the CTOD exceeds 5 μm, when a controlling J-dominated region is established.

Sharpe *et al.* (1988) assumed that the loading rate $\dot{K}_I$ was constant and the CTOD was a direct measure of the stress intensity factor during the experiment, allowing them to use the ASTM E 399 5% offset method on the CTOD versus time curve to determine the fracture toughness. In Fig. 14, the stress intensity factor K_I is plotted versus normalized time for the precracked rate sensitive and rate independent models. Evidently, their assumption of a constant $\dot{K}_I$ is valid since the loading rate is approximately 7×10^6 MPa m$^{1/2}$ s^{-1} and remains fairly constant after the loading starts to open the crack. However, they also assume that the stress intensity factor K_I is linearly related to the CTOD, which is a much weaker assumption (See Fig. 13).

The rate independent and quasi-static analyses produce J-integral versus CTOD curves (Fig. 13) that are very close. However, the contours of von Mises surface stress for the two analyses are different (Fig. 17) at 15 μs or a CTOD = 11.5 μm. In Fig. 17, the dashed lines emanate from the crack tip and pass through the maximum extent of each plastic stress contour line. The angle between the dashed lines and the dotted line θ_s (from the quasi-static response) is greater than θ_d (from the dynamic rate insensitive response). On the other hand, the near tip stresses are very close inside a radius of ~ 100 μm.

The difference between the static and rate independent surface may be accounted for by the effect of the T-stress (Larsson and Carlsson, 1973), which is a uniform non-singular stress acting parallel to the crack faces in the direction of the crack in mode I. A similar stress term was used by Irwin (1958) in his numerical analysis of an experiment by Wells and Post (1958) involving the photoelastic analysis of running cracks. Rice (1974), using

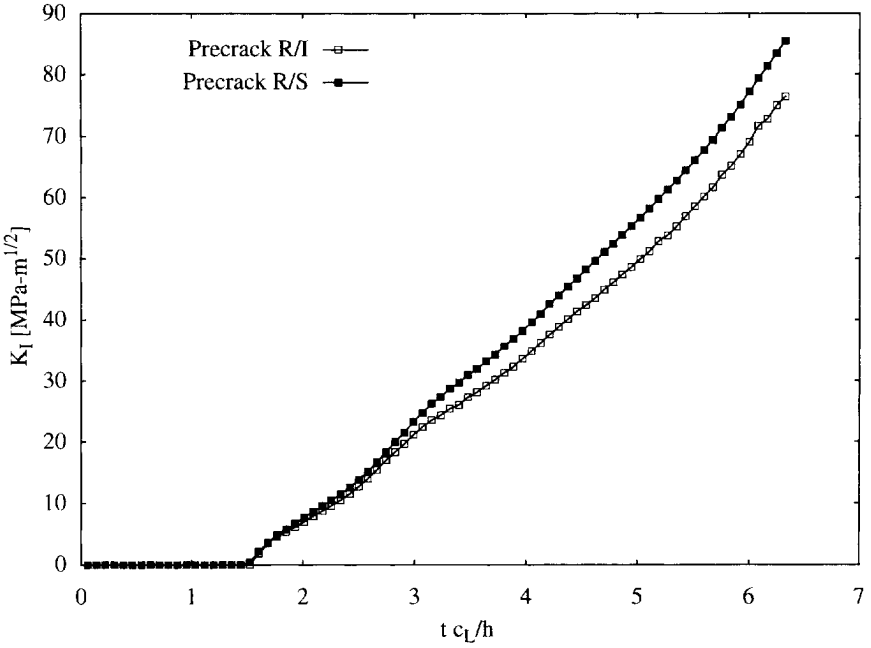

Fig. 14. The dynamic stress intensity factor versus normalized time for the precracked rate sensitive and rate independent analyses. The loading rate of 7×10^6 MPa m$^{1/2}$ s^{-1} is fairly constant after 3 tc_L/h, and is approximately 15% greater than loading rate of the rate independent model.

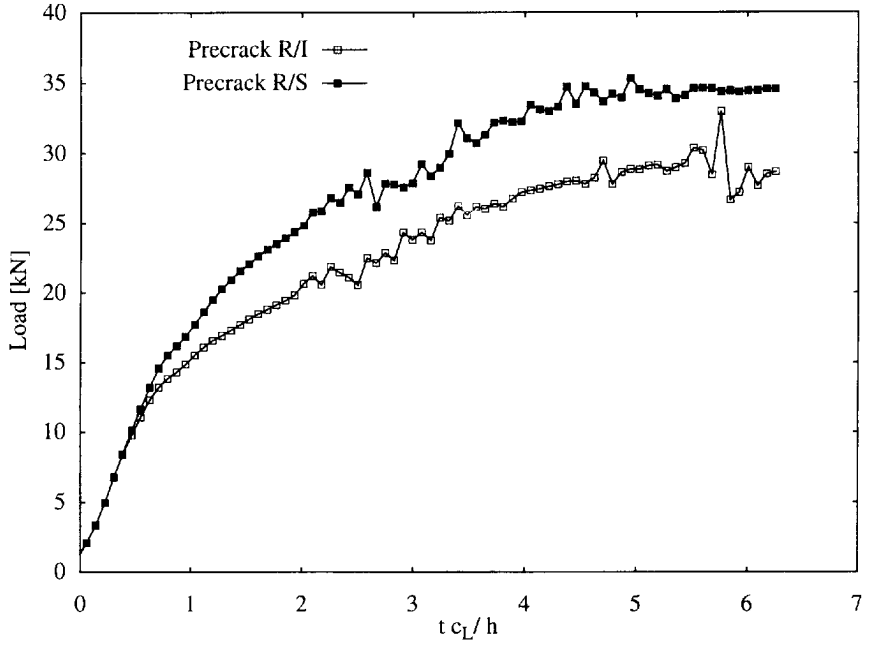

Fig. 15. The dynamic tup load versus normalized time for precracked strain-rate independent and sensitive models. The maximum load is approximately 10 times that of the quasi-static maximum load.

the two-dimensional expansion of the asymptotic stress fields around a crack tip, defined the T-stress as

$$\begin{bmatrix} \sigma_{xx} & \sigma_{xy} \\ \sigma_{xy} & \sigma_{yy} \end{bmatrix} = \frac{K}{\sqrt{r}} \begin{bmatrix} f_{xx}(\Theta) & f_{xy}(\Theta) \\ f_{xy}(\Theta) & f_{yy}(\Theta) \end{bmatrix} + \begin{bmatrix} T & 0 \\ 0 & 0 \end{bmatrix} + \text{higher order terms}, \tag{3}$$

σ_{ij} are the Cartesian stress components, K is the mode I stress intensity factor, r is the

Contour Line	σ_{yy} (GPa)
A	0.0
B	0.2
C	0.4
D	0.6
E	0.8
F	1.0

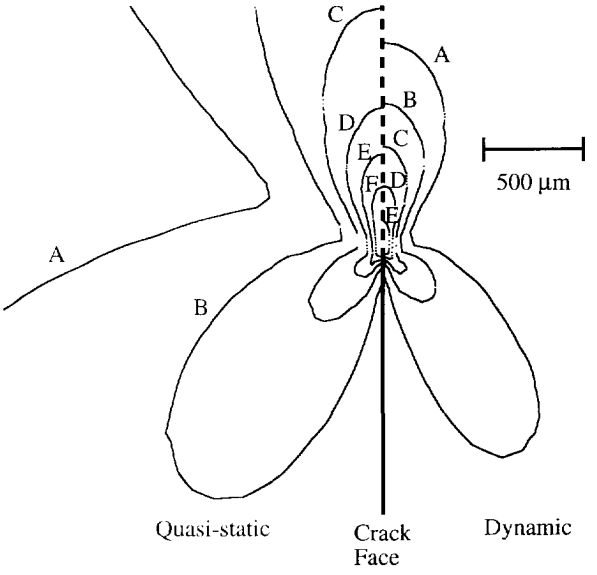

Fig. 16. The contours of σ_{yy} on the surface of the specimen around the crack tip for quasi-static (left) and dynamic rate independent (right) analyses at CTOD = 11.5 μm (time = 15.4 μs). The static model has a larger T-stress.

Contour Line	Mises Stress (GPa)
A	0.4
B	0.6
C	0.8
D	1.0
E	1.2
F	1.4
G	1.6

σ_y = 1.5 GPa

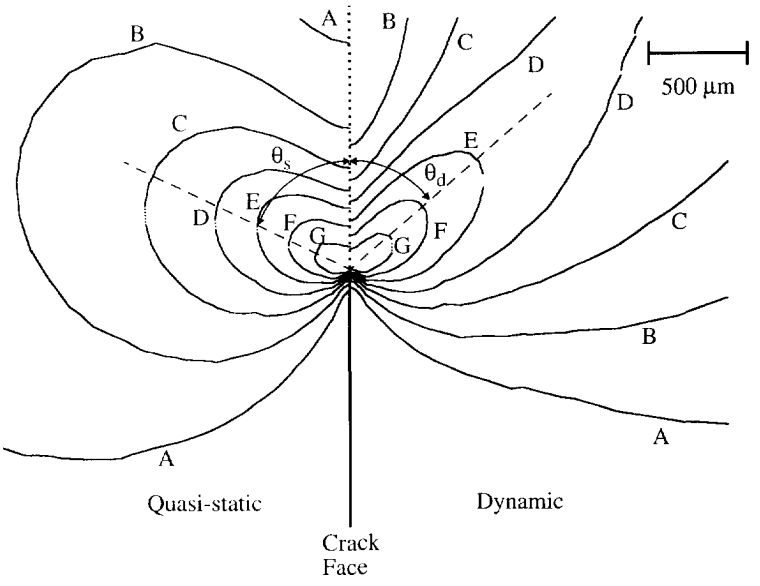

Fig. 17. The contours of von Mises stress on the surface of the specimen around the crack tip for the quasi-static (left) and rate independent dynamic (right) analyses at CTOD = 11.5 μm (time = 15.4 μs). The larger T-stress causes the contour lobes to rotate toward the crack face, i.e. $\theta_s < \theta_d$.

distance from the crack tip, Θ is the angle from the crack, the functions $f_{ij}(\Theta)$ are given by the elastic solution and T is the T-stress. Rice showed that the T-stress controls the orientation of the plastic stress contours with the crack faces. The larger the T-stress, the larger Θ becomes. A comparison of the stresses acting parallel to the crack faces for the quasi-static and strain rate independent models for the same CTOD of 11.5 μm is shown in Fig. 16, where the σ_{yy} contour lines are shown for the quasi-static and rate independent models on the left and right of the crack face, respectively. The shapes and locations of contour lines labeled D, E and F from the quasi-static model are very close to the shapes and locations of contour lines labeled B, C and D from the dynamic model, indicating that the quasi-static model has a superimposed σ_{yy} of 0.4 MPa larger than the dynamic model that is uniform around the crack tip. The difference in the J-integral versus CTOD curves

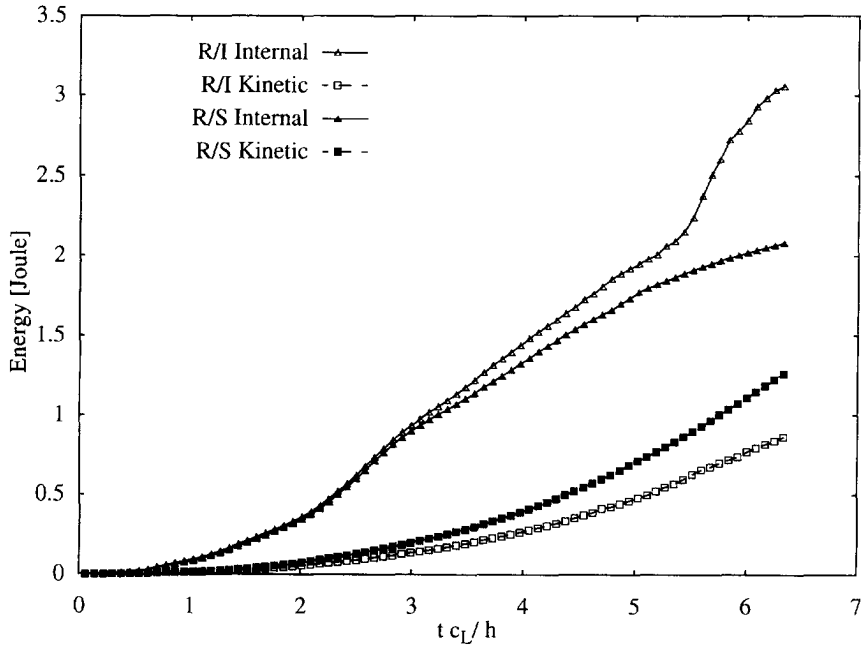

Fig. 18. The internal and kinetic energy versus normalized time for precracked, dynamic rate sensitive and independent models. The test ends before the transition time (Nakamura *et al.*, 1985a).

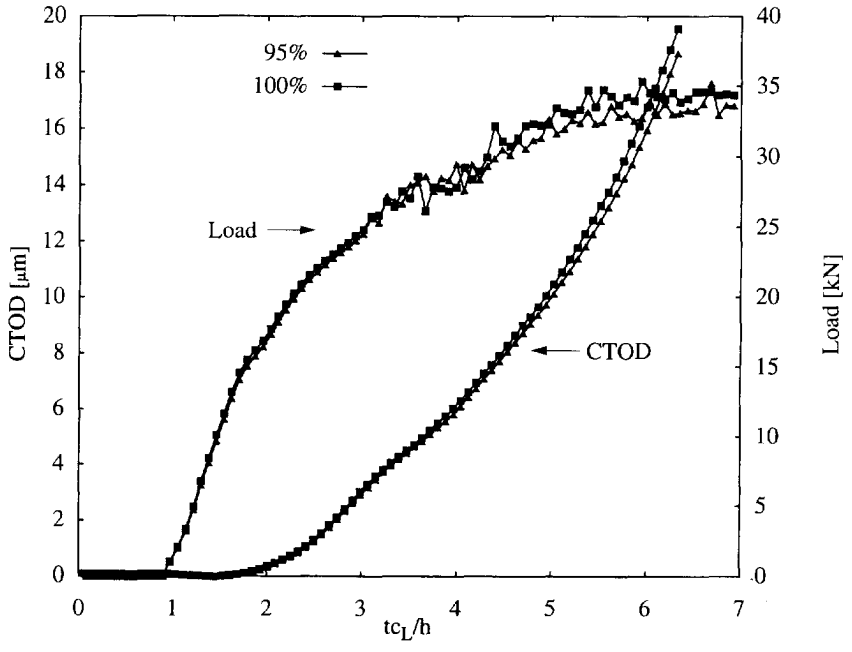

Fig. 19. The effect of projectile speed on dynamic CTOD versus normalized time. The larger the projectile speed, the earlier the maximum load will be applied to the specimen.

for the quasi-static and rate independent models (Fig. 13) can also be explained by the T-stress effect. Following Rice (1974) again, the T-stress has no effect on the J-integral, but it does affect the CTOD. Larger values of the T-stress will produces smaller CTOD values for a fixed value of the J-integral. For a given value of the J-integral greater than 10 kPa m (Fig. 13), the CTOD for the quasi-static model is less than the CTOD for the rate independent model, because the quasi-static model has a larger T-stress than the rate independent model (Fig. 16).

The effects of the projectile velocity and tup contact area are shown in Figs 19 and 20, respectively. Figure 19 shows the response of the CTOD and contact load versus normalized

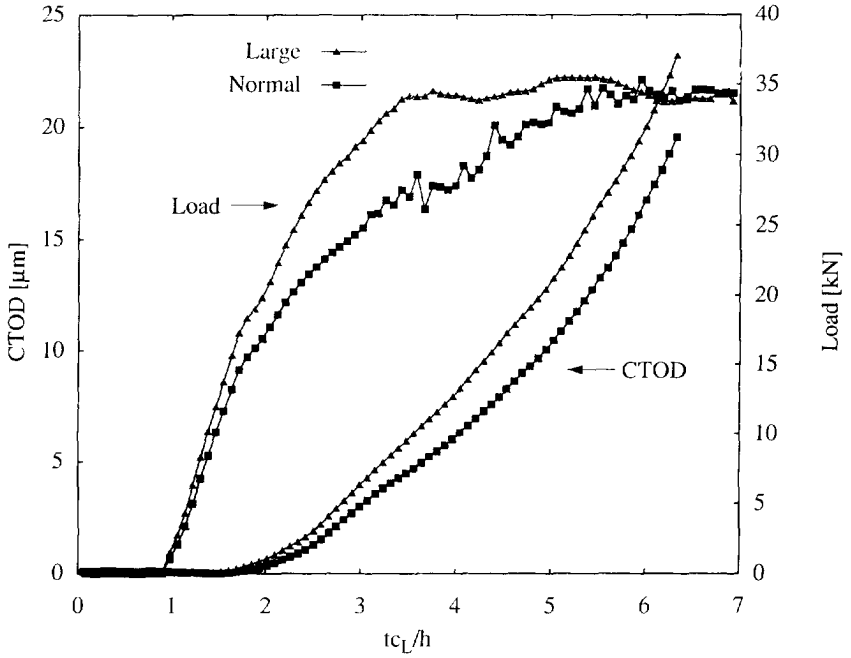

Fig. 20. The effect of tup contact area on the CTOD and a dynamic load for precracked rate sensitive model. The large tup had a 50% larger contact area than the tup used in the experiment. The tup contact area controls the maximum dynamic load.

time for two projectile velocities. A 5% decrease in the projectile speed causes a negligible change in the CTOD and load. Figure 20 shows the response of the CTOD and contact load versus normalized time for two tup areas. A 50% increase in the tup areas causes a 30% increase in the CTOD after $\sim 4\ tc_L/h$. The larger tup also increases the rate at which the maximum load is attained.

5. CONCLUSIONS

Three-dimensional, dynamic, rate sensitive, elastic plastic finite element analyses of an impact fracture toughness test of a 3PB specimen of 4340 steel were performed in order to determine the effect of impact loading rates on the initiation fracture toughness of 4340 steel. As a measure of the fidelity of the simulation the observed CTOD, as measured 100 μm behind the crack tip, was compared with computed values. The finite element simulations were used to obtain local crack field quantities (such as the J-integral) and estimate the fracture initiation time.

The effects of the residual plastic stresses and curved crack front due to the fatigue precrack on the CTOD were modeled by growing a crack in the finite element model before applying the impact load. The analyses showed that the finite element model which accounted for rate sensitive material behavior correlated very well with the observed dynamic CTOD versus time curve and that there was no indication of fracture initiation in the experimentally observed 10 μs. A rate independent analysis was also in reasonable agreement with the observed CTOD, but produced a J-integral $\sim 25\%$ lower than the rate sensitive model. These finite element analyses show that the time evolution of the J-integral is affected by the rate sensitivity of the material. More importantly, while the quasi-static J-integral was 11 kPa m at initiation (as defined by ASTM E 399), in the impact loaded 3PB specimen, the fracture toughness, as measured by the J-integral, is at least 25 kPa m.

Since the CTOD is measured so close to the crack tip (100 μm back from the surface crack) it is within a region that becomes dominated by the local crack tip fields at a time of $\sim 2\ tc_L/h$. While this CTOD measurement is not a direct measure of these HRR fields, it is in the J-dominated zone since the J-integral is very close to linear in CTOD. If the 4340 steel is assumed to be rate independent, than a quasi-static analysis could be used to

determine the J-integral from the dynamic CTOD; however, the finite element analyses done here show that the T-stress in the quasi-static finite element model is greater than that found in the rate independent dynamic model. The T-stress changes the shape of the of the plastic zone around the crack tip and affects the CTOD for a given J-integral.

The finite element analyses presented here provide a useful tool for guiding further experiments of the type performed by Tregoning *et al.* (1992). If observation of the CTOD is to be used in conjunction with a finite element simulation to obtain local field information, including the J-integral, then the indents should be placed further back from the crack tip to provide more than an order of magnitude more CTOD than the resolution of the measuring device (such as the ISDG) while still remaining inside the J-dominated region. This will enhance the accuracy of the measurements and minimize any inaccuracies in the modeling of the precrack and due to the three-dimensional effects very near the crack tip.

Once the correlation of the finite element model and the experiment had been established, the observation point (in this case the ISDG indents) could then be moved very close to the crack tip to use them to detect fracture initiation in much the same way as strain gages have been used to measure the time at which fracture initiation occurs. In these 3PB experiments, the projectile speed and tup contact area controlled how fast the maximum applied load was attained and therefore the loading rate.

Acknowledgements—The assistance of Brad Maker with NIKE3D, Robert Whirley with DYNA3D, Tom Spelce with Taurus and Mark Christon with Ingrid is appreciated. The use of Ed Zywick's J-integral post-processor is also appreciated.

REFERENCES

American Society of Testing and Materials (1983). E 399 83 Standard test method for plane-strain fracture toughness of metallic materials.

Andersson, H. (1975). The steadily growing, elastic–plastic crack tip in a finite element treatment. *Int. J. Fracture* **9,** 231–233.

Aoki, S., Kishimoto, K. and Sakata, M. (1980). On the path independent integral. *J. Engng Fracture Mech.* **13,** 841–850.

Aoki, S., Kishimoto, K. and Sakata, M. (1984). Energy flux into process region in elastic–plastic fracture problems. *Engng Fracture Mech.* **19,** 827–836.

Atluri, S. N. (1982). Path independent integrals in finite elasticity and inelasticity, with body force, inertia, and arbitrary crack-face conditions. *Engng Fracture Mech.* **16,** 341–364.

Begley, J. A. and Landes, J. D. (1972). The J integral as a fracture criterion. *Fracture Toughness, Proceedings of the* 1971 *National Symposium on Fracture Mechanics, Part II, ASTM STP* **514,** 1–20, Philadelphia.

Belytschko, T. (1983). An overview of semidiscretization and time integration procedures. In *Computational Methods for Transient Analysis* (Edited by T. Belytschko and T. J. R. Hughes), Vol. 1, pp. 1–63. North-Holland, New York.

Chi, Y. C., Cho, K. and Duffy, J. (1989). The effect of tempering and test temperature on the dynamic fracture initiation behavior of an AISI 4340 VAR steel. *Mater. Sci. Engng* **A114,** 105–126.

Christon, M. A. and Dovey, D. (1992). INGRID A 3-d mesh generator for modeling nonlinear systems. UCRL-MA-109790, Lawrence Livermore National Laboratory.

Costin, L. S., Duffy, J. and Freund, L. B. (1976). *Fracture Initiation in Metals Under Stress Wave Loading Conditions* (Edited by G. T. Hahn and E. M. F. Kanninen), *ASTM STP* **627,** 301–318.

deLorenzi, H. G. (1982). On the energy release rate and the J-integral for 3-D crack configurations. *Int. J. Fracture* **19,** 183–193.

Douglas, A. S. and Suh, M. S. (1990). Impact fracture on a tough ductile steel. *Fracture Mechanics: Twenty-First Symposium* 1074 (Edited by J. P. Gudas, J. A. Joyce and E. M. Hackett), pp. 109–125.

Elber, W. (1970). Fatigue crack closure under cyclic tension. *Engng Fracture Mech.* **2,** 37–45.

Giovanola, J. H. J. (1985). Fracture toughness testing using servohydraulic testing systems. In *Metal Handbook, Vol. 8, Mechanical Testing*, pp. 259–261. ASM, Ohio.

Godse, G., Ravichandran, G. and Clifton, J. (1989). Micromechanics of dynamic crack propagation in an AISI 4340 steel. *Mater. Sci. Engng* **A112,** 79–88.

Hackett, E. M., Joyce, J. A. and Shih, C. F. (1987). Measurement of dynamic fracture toughness of ductile materials. DTNSRDC SME-87-07. David W. Taylor Naval Ship Research and Development Center.

Hellen, T. K. (1975). On the method of virtual crack extension. *Int. J. Numer. Meth. Engng* **9,** 187–207.

Homma, H., Shockey, D. A. and Murayama, Y. (1983). Response of cracks in structural materials to short pulse loads. *J. Mech. Phys. Solids* **31,** 261–279.

Hutchinson, J. W. (1968). Singular behaviour at the end of a tensile crack in a hardening material. *J. Mech Phys. Solids* **16,** 13–31.

Irwin, G. (1958). Discussion of the dynamic stress distribution surrounding a running crack—a photoelastic analysis. *Proc. Soc. Exp. Stress Anal.* **16,** 93–96.

Kanninen, M. F. and Popelar, C. H. (1985). *Advanced Fracture Mechanics*. Oxford University Press, New York.

Kobayashi and Yung (1988). A hybrid technique for high-temperature dynamic fracture analysis. In *Application of Advanced Strain Measurement Techniques*. British Society for Strain Measurement, Whittles Publishing, Caithness.

Kobayashi, A. S., Chiu, S. T. and Beeuwkes, R. (1973). A numerical and experimental investigation on the use of *J*-integral. *Engng Fract. Mech.* **5,** 293–305.

Krishnaswamy, S., Rosakis, A. J. and Ravichandran, G. (1988). On the extent of dominance of asymptotic elastodynamic crack-tip fields; part II: numerical investigation of three-dimensional and transient effects. *J. Appl. Mech.* **58,** 99–103.

Larsson, S. G. and Carlsson, A. J. (1973). Influence on non-singular stress terms and specimen geometry on small-scale yielding at crack tips in elastic–plastic materials, *J. Mech. Phys. Solids* **21,** 263–277.

Lee, Y. J. and Freund, L. B. (1990). Fracture initiation due to asymmetric impact loading of an edge cracked plate. *J. Appl. Mech.* **57,** 104–111.

Maker, B. N. (1991). NIKE3D A nonlinear, implicit, three-dimensional finite element code for solid and structural mechanics—user's manual. UCRL-MA-105268, Lawrence Livermore National Laboratory.

Matthies, H. and Strang, G. (1979). The solution of nonlinear finite element equations. *Int. J. Numer. Meth Engng* **14,** 1613–1626.

McClung, R. C. and Sehitoglu, H. (1989a). On the finite element analysis of fatigue crack closure—1. Basic modelling issues. *Engng Fracture Mech.* **33,** 237–252.

McClung, R. C. and Sehitoglu, H. (1989b). On the finite element analysis of fatigue crack closure—2. Numerical results. *Engng Fracture Mech.* **33,** 253–272.

Merkel, J. G., Paris, P. C. and Rice, J. R. (1973). Some further results of *J*-integral analysis and estimates. *ASTM STP* **536,** 231–245.

Nakamura, T., Shih, C. F. and Freund, L. B. (1985a). Elastic–plastic analysis of a dynamically loaded circumferentially notched round bar. *Engng Fracture Mech.* **22,** 437–452.

Nakamura, T., Shih, C. F. and Freund, L. B. (1985b). Computational methods based on an energy integral in dynamic fracture. *Int. J. Fracture* **27,** 229–243.

Nakamura, T., Shih, C. F. and Freund, L. B. (1986a). Analysis of a dynamically loaded three-point-bend ductile fracture specimen. *Engng Fracture Mech.* **25,** 323–339.

Nakamura, T., Shih, C. F. and Freund, L. B. (1986b). Three-dimensional transient analysis of a dynamically loaded three-point-bend ductile fracture specimen. ONR0365/3 Office of Naval Research.

Newman, J. C., Jr (1976). A finite-element analysis of fatigue crack closure. *Mech. Crack Growth* **590,** 281–301.

Parks, D. M. (1977). The virtual crack extension method for nonlinear material behavior. *Comput. Meth. Appl. Mech. Engng* **12,** 353–364.

Premack, T. and Douglas, A. S. (1993). An analysis of the crack tip fields in a ductile three-point bend specimen subjected to impact loading. *Engng Fracture Mech.* **45,** 717–728.

Ravichandran, G. and Clifton, R. (1989). Dynamic fracture under plane wave loading. *Int. J. Fracture* **40,** 157–201.

Rice, J. R. (1968). A path independent integral and the approximate analysis of strain concentration by notches and cracks. *J. Appl. Mech.* **34,** 379–386.

Rice, J. R. (1974). Limitations to the small scale yielding approximation for crack tip plasticity. *J. Mech. Phys. Solids* **22,** 17–26.

Rice, J. R. and Rosengren, G. F. (1968). Plane strain deformation near a crack tip in a power-law hardening material. *J. Mech. Phys. Solids* **16,** 1–12.

Sakata, M., Aoki, S., Kishimoto, K. and Takagi, R. (1983). Distribution of crack extension force, the *J*-integral, along a through-crack-front of a plate. *Int. J. Fracture* **23,** 187–200.

Shapiro, J. M. (1987). An experimental method for determination of dynamic fracture toughness. Ph.D. Thesis, Johns Hopkins University, Baltimore, Maryland.

Sharpe, W. N., Jr (1970). Dynamic strain measurement with the interferometric strain gage. *Exp. Mech.* **10,** 89–92.

Sharpe, W. N., Jr, Douglas, A. S. and Shapiro, J. M. (1988). *WNS/ASD*-88-02. The Johns Hopkins University, Baltimore, Maryland.

Shih, C. F. (1981). Relationship between the *J*-integral and the crack opening displacement for stationary and extending cracks. *JMPS* **29,** 305–326.

Shih, C. F., Moran, B. and Nakamura, T. (1986). Energy release rate along a three-dimensional crack front in a thermally stressed body. *Int. J. Fracture* **30,** 79–102.

Spelce, T. (1991). TAURUS: An interactive post-processor for the analysis codes NIKE3D, DYNA3D, and TOPAZ3D. UCRL-MA-105401, Lawrence Livermore National Laboratory.

Syracuse University Research Institute (1963). *Aerospace Structural Metals Handbook*. Syracuse University Press, Syracuse.

Thau, S. A. and Lu, T. H. (1971). Transient stress intensity factors for a finite crack in an elastic solid caused by a dilatational wave. *Int. J. Solids Structures* **7,** 731–750.

Tracy, D. M. (1976). Finite element solutions for crack-tip behavior in small-scale yielding. *J. Engng Mater. Tech.* **98,** 146–151.

Tregoning, R. L., Shapiro, J. M. and Sharpe, W. N., Jr (1992). Dynamic CTOD measurements with applications to fracture toughness testing. In *Rapid Load Fracture Testing* 1120 (Edited by R. Chonan and W. R. Corwin), pp. 119–133. American Society of Testing Procedures, Philadelphia.

Wells, A. A. and Post, D. (1958). The dynamic stress distribution surrounding a running crack—a photoelastic analysis. *Exp. Stress Anal.* **16,** 69–96.

Whirley, R. G. (1991). DYNA3D A nonlinear, explicit, three-dimensional finite element code for solid and structural mechanics—user manual. UCRL-MA-105254, Lawrence Livermore National Laboratory.

Yokoyama, T. and Kishida, K. (1988). Measurement of dynamic fracture initiation toughness by a novel impact three-point bend test technique using Hopkinson pressure bars. In *Impact Loading and Dynamic Behavior of Materials*. (Edited by C. Y. Chiem, H.-D. Kunze and L. W. Meyer), pp. 273–280. DGM Informationsgesellschaft Verlag, Oberursel.

Zehnder, A. T. and Rosakis, A. J. (1990). Dynamic measurement of the *J*-integral in ductile metals: comparison of experimental and numerical techniques. *Int. J. Fracture* **42,** 209–230.